



## Encapsulation of Cu(II), Ni(II) and V(IV) - imidazole complexes in fly ash zeolite, characterisation and catalytic activity towards hydroxylation of phenol

S. Sheeba Thavamani and T. Peter Amaladhas\*

*P.G and Research Department of Chemistry, V.O. Chidambaram College, Tuticorin - 628008, Tamil Nadu, India.*

*Received 10 Sep 2015, Revised 18 Dec 2015, Accepted 28 Dec 2015*

*\*Corresponding author: E-mail: [peteramaldhast@yahoo.co.in](mailto:peteramaldhast@yahoo.co.in); Phone: +91 9442210876; Fax: +91 461 2310275*

### Abstract

In this article, a new method for the utilization of fly ash has been proposed. X-type zeolite was prepared from fly ash by alkali fusion followed by hydrothermal method. The prepared fly ash based zeolite (FAZ) was characterised using FTIR, XRD, TGA and XRF and from BET analysis the surface area was found to be 172.83 m<sup>2</sup>/g and the pore volume was 0.014 cm<sup>3</sup>/g. Cation Exchange Capacity (CEC) of raw fly ash was found to be 0 meq/100g while that of FAZ was estimated to be 457 meq/100g. The increase in surface area and CEC confirms zeolitisation. Cu(II), Ni(II) and V(IV) - imidazole complexes were encapsulated in FAZ using flexible ligand method. The FAZ encapsulated with complexes were characterised by FT-IR, XRD, UV-Vis, AAS and TGA. The C=N stretching frequency observed at 1068 cm<sup>-1</sup> and N-H stretching observed at ~3419 cm<sup>-1</sup> clearly indicate the loading of metal-imidazole complexes in the pores of fly ash zeolite. Thermo grams of the metal complexes encapsulated fly ash zeolite shows an additional weight loss at 200-500°C which confirms the loading of metal complexes in zeolite. X-Ray diffraction patterns of the encapsulated metal complexes remain unaffected due to poor loading of the metal complexes in the pores of zeolite. Hydroxylation of phenol has been chosen as a model reaction and the catalytic activity of the encapsulated complexes towards this reaction has been monitored as a function of time. The results reveal up to 81.8% conversion of phenol to hydroquinol which has been characterised by GC-MS.

**Keywords:** Zeolite, Fly ash, Fly ash based zeolite, Flexible ligand method, Imidazole

### 1. Introduction

Disposal of fly ash is a major issue worldwide, particularly in India because the major source of electricity generation in India is coal-based. The total installed capacity in India is 80458 MW and 131.09 million-tonne of ash is generated every year and it is expected to increase to 300-400 MT/year by 2016-17 [1]. A large number of technologies have been developed for gainful utilization and safe management of fly ash. As a result, the utilization of fly ash has increased to over 73 million tonne in 2010-12. Fly ash was moved from “hazardous industrial waste” to “waste material” category during the year 2000 and during November 2009, it became a saleable commodity. Fly ash utilization has started gaining acceptance, it being 55.79% during 2010-12. Fly ash has acquired the status of a “useful commodity” which opens up plenty of opportunities in terms of laying and fine tuning policies, conducting gainful businesses and R&D efforts, and addressing the concerns of environment at the same time. Though a considerable amount of fly ash has been utilised, a lot of efforts are required to reach the target of 100% ash utilization. This method of fly ash utilization provides an innovation in technology and solution development and serves a good purpose to guide further strategies that turns the “menace” into a “meaningful” engagement and utilisation of fly ash.

Zeolites are aluminosilicates that are formed by the mutual sharing of oxygen atoms between tetrahedra of silica and alumina. Apart from naturally occurring zeolites, a number of synthetic zeolites are known which have a wide range of applications including ion exchange, catalysis, gas masks, in nuclear and biogas industries, in construction, agriculture and biomedical applications. Encapsulation of suitable molecular species in zeolitic cavities to prepare a new variety of materials has gained interest in the field of research. They have been reported to have applications in size and shape selective catalysis, gas separation and purification and in photocatalysis [2-4]. They have a fascinating role in heterogeneous catalysis claiming stereoselectivity, easy recovery of products and reusability of the catalyst [5]. In this work, we report (i) the synthesis and characterisation of zeolite from fly ash, (ii) encapsulation of Cu(II), Ni(II) and V(IV) complexes of imidazole in fly ash based zeolite and their characterization and (iii) assessment of the FAZ encapsulated complexes as catalysts towards the hydroxylation of phenol as a function of time.

## 2. Experimental

### 2.1. Materials

The main raw material, F-type coal fly ash sample was collected from electrostatic precipitators of Tuticorin Thermal Power Station (TTPS), Tuticorin, Tamil Nadu, India. The sample contained both amorphous (mainly SiO<sub>2</sub> and Al<sub>2</sub>O<sub>3</sub>) and crystalline components (mainly quartz and mullite). AR Grade concentrated Hydrochloric acid supplied by Ranbaxy India was used for the acid treatment of fly ash. Sodium hydroxide used for zeolite synthesis was purchased from Fisher, India, min. assay 98.0%. AR grade, 99% pure, E Merck make, Cupric Nitrate (Cu(NO<sub>3</sub>)<sub>2</sub>·3H<sub>2</sub>O), Nickel Nitrate (Ni(NO<sub>3</sub>)<sub>2</sub>·6H<sub>2</sub>O) and Ottokemi, Mumbai, India make, 98% pure, VO(H<sub>2</sub>O)<sub>4</sub>SO<sub>4</sub> were used for preparing metal exchanged zeolites. AR grade Imidazole of 99.9% purity, supplied by Fischer, Chennai, India was used for the synthesis of encapsulated metal-imidazole complexes. Phenol of assay 99.0% purchased from Chemspure, Chennai, India was used for catalytic studies. Acetonitrile and dichloromethane (HPLC grade) of 99.5% purity were used as solvents. 40% solution of HF (Sigma-Aldrich) was used to dissolve the zeolite encapsulated metal complexes for AAS analysis. E Merck make, Hydrogen peroxide solution of assay 30-32% W/V was used to study the catalytic activity of the encapsulated metal complexes towards the hydroxylation of phenol. The H<sub>2</sub>O<sub>2</sub> solution was kept in a dark polyethylene bottle preserved in a refrigerator to retard decomposition.

FTIR spectra were recorded as KBr pellet on a SHIMADZU FTIR 8400S spectrophotometer in the frequency range 400-4000 cm<sup>-1</sup> with a resolution of 0.1 cm<sup>-1</sup>. The structural crystallinity of the encapsulated complexes was confirmed by recording the XRD patterns in PANalytical model X'pert PRO using CuK $\alpha$  (2.2 KW Max.) source and X'celerator (semiconductor) detector. Ni filtered CuK $\alpha$  radiation was used with a curved graphite crystal monochromator and NaI scintillator. Data were collected in the 2 $\theta$  range 10-80 degrees at a 2 $\theta$  step size of 0.05. Thermo grams of the zeolite and the encapsulated metal complexes were recorded on Perkin- Elmer model-TGA7 instrument with a vertical furnace and vertical sample gas flow at a heating rate of 10<sup>0</sup>C per minute in nitrogen atmosphere by taking 5 mg of the sample. A known weight of the encapsulated complex was taken in a Platinum crucible with lid and heated from 50<sup>0</sup>C to 860<sup>0</sup>C to monitor the weight loss on heating in each stage. UV-Vis spectra were recorded from 190 to 1000 nm using JASCO, V-530 model spectrophotometer after leaching the encapsulated metal complexes. For this, 25 mg of metal complex encapsulated zeolite was heated with 20 mL of dilute sulphuric acid to facilitate leaching of the metal complex. The metal contents in the zeolite encapsulated metal complexes were measured using Varian, Model Spectraa 220 Atomic Absorption Spectrometer in the flame of acetylene-air mixture. 50 mg of the encapsulated metal complex was dissolved in 20 mL of HF (40%) and the metal contents in the solution were analysed using Atomic Absorption Spectrometer. To study the surface morphology, SEM images were recorded using Quanta 200, FEI SEM instrument. GC analysis was carried out to identify the products obtained from the metal complexes encapsulated zeolite catalysed hydroxylation of phenol with H<sub>2</sub>O<sub>2</sub> in Hewlett Packard GC-MS, HP 5890 instrument fitted with FID detector and RTX 502.2 column of length 60 m, 0.25 ID using He as the carrier gas. (Temperature program: Initial Temperature 70<sup>0</sup>C for 12 minutes and increased at the rate of 10<sup>0</sup>C per min up to a temperature of 250<sup>0</sup>C. Injection volume - 0.5 microlitre). The composition of fly ash and FAZ were determined by X-ray fluorescence spectrometry (XRF) on a Philips

MAGIX PRO Model 2440 instrument. The sample was additionally pulverised, homogenised and pressed into pellet with chromatographic cellulose as binder for the analysis. BET surface analysis was carried out on a Carlo-Erba sorptometer, Model 1800. Prior to the adsorption measurements, the sample was outgassed at 373K for 12 h, in high vacuum. After evacuation, the sample was cooled at room temperature and weighed. For analysis, the sample was cooled to 78K using liquid Nitrogen and then Nitrogen was allowed to adsorb on them. The volume of Nitrogen adsorbed (at STP) and the BET surface areas were then measured. Surface area and pore volume were obtained from N<sub>2</sub> adsorption–desorption isotherms using conventional BET and BJH methods.

### 2.2. Zeolite synthesis

Fly ash was collected from the electrostatic precipitators of Tuticorin Thermal Power Station (TTPS) and used for this study. X-type zeolite was synthesized from F-type fly ash by hydrothermal method [6]. In a typical experiment, the raw fly ash sample was first screened through a sieve of 80-mesh size, to eliminate the larger particles. The unburnt carbon (3%) along with other volatile materials present in fly ash were removed by calcination at 800(±10°C) for 2 hours. The calcined fly ash sample was further treated with hydrochloric acid to increase its activity towards zeolite formation and to remove iron oxides. The treated fly ash was milled with NaOH in the ratio 1:1 and fused for one hour at 550°C in a muffle furnace. The resultant fused mixture was cooled and milled again. It was then mixed with a calculated amount of distilled water and stirred continuously for 8 hours in a mechanical stirrer. The mixture was then left undisturbed for 6 hours at 90°C. Finally it is filtered, washed repeatedly with distilled water, dried at 110°C and kept in powder form for further procedures.

### 2.3. Determination of cation exchange capacity of the prepared zeolite

The synthesised zeolite sample was first dried at 240°C for an hour to remove water molecules. Exactly 0.5 g of this dried zeolite sample was transferred to a beaker containing 200 mL of 0.05% CaCl<sub>2</sub> solution. The mixture was stirred using a magnetic stirrer for 15 min to facilitate the sample to perform exchange of Ca<sup>2+</sup> ions. The mixture was then filtered using sintered G-4 glass crucible. The filtrate (40 mL) and 200 mL of the stock CaCl<sub>2</sub> solutions were titrated with 0.005 M EDTA solution separately using 2 mL of NH<sub>3</sub>-NH<sub>4</sub>Cl buffer and 2 drops of Eriochrome Black T indicator. The end point is the colour change from wine red to blue. The difference in titre values, gives the amount of Ca<sup>2+</sup> exchanged with zeolite. The cation exchange capacity (meq/100) is calculated using the following equation:

$$CEC = \frac{\text{Volume of EDTA} \times \text{Strength of EDTA}}{\text{Weight of zeolite taken}} \times 100 \times \frac{200}{40}$$

### 2.4. Preparation of metal complexes encapsulated zeolites by flexible ligand method

The metal complex encapsulated zeolites were prepared by flexible ligand method. The metal ion was exchanged with the Na<sup>+</sup> ions of the FAZ which were further treated with the ligand. In this approach, the flexible ligand must be able to diffuse freely through the zeolite pores, where it coordinated to the previously exchanged transition metal cations to form the metal complex which is too large to exit. The zeolite encapsulated metal complexes were Soxhlet extracted with a suitable solvent to remove any uncomplexed ligand and metal complexes adhered to the surface of the zeolite. Soxhlet extraction has been performed for several hours and the extracted solvent was found to be colourless which indicated the complete removal of the metal complex from the surface. Residual colours that have been noticed in all the zeolite encapsulated metal complexes were due to the loading of the metal complex in the cages of the zeolite.

#### 2.4.1. Preparation of metal exchanged zeolite, M-X; [M = Cu(II), Ni(II) and V(IV)]

About 1.0 g of fly ash zeolite (FAZ) was suspended in 100 mL of 0.1 M metal salt solution (Nitrates of Cu(II), Ni(II) and Vanadyl sulphate). The reaction mixture was magnetically stirred for 24 hours. The solid was filtered, washed with distilled water till the filtrate was free from the metal ion on the surface of the zeolite and then dried for 15 hours at 150°C in an air oven. The Cu(II) – X and Ni(II) - X were pale green in colour and V(IV) - X was

dark green in colour. This colour change may be attributed to the metal ions that have been exchanged for the Na<sup>+</sup> ions of the zeolite matrix.

#### 2.4.2. Preparation of metal-imidazole complexes encapsulated zeolite [M(IMD)-X]

Imidazole (2.5 g) and 1.0 g of metal ion exchanged zeolite [M= Cu(II), Ni(II) or V(IV)] were mixed in 50 mL acetonitrile in a flat bottomed flask and the reaction mixture was heated at reflux for ca.15 hours while stirring magnetically. After cooling, the slurry was Soxhlet extracted with dichloromethane (ca.48 hours) by circulating ice cooled water in the condenser. The extraction was continued till the complex was free from unreacted ligand and any free metal complex on the surface of the zeolite. The encapsulated Cu(II), V(IV) and Ni(II) complexes of imidazole were blue, green and pale green respectively. The coloured solids were dried at 150<sup>0</sup>C for five hours till constant weight was achieved.

#### 2.5. Catalytic activity studies of encapsulated metal complexes of imidazole

The suitability of the encapsulated metal complexes as catalysts in phenol hydroxylation as a model reaction was assessed. In a typical reaction, an aqueous solution of 30% H<sub>2</sub>O<sub>2</sub> (1.6 mL, 53.38 mmol) and phenol (0.54 g, 6.16 mmol) were mixed in 5 mL CH<sub>3</sub>CN. Zeolite encapsulated metal imidazole complex (M(IMD)-X) (0.020g) was added to the reaction mixture and was refluxed for the stipulated time. The products were analyzed by GC-MS and identified to be hydroquinol. The amount of unreacted phenol in the reaction mixture was estimated quantitatively by substituting with bromine produced from bromide and bromate in acid solution. The unreacted bromine was determined by adding excess potassium iodide and back titrating the liberated iodine with standard sodium thiosulphate solution [7, 8].

### 3. Results and discussion

#### 3.1. Characterization of the prepared fly ash zeolite (FAZ)

##### 3.1.1. Cation exchange capacity

The major potential application of zeolite is based on its use as ion exchangers in industrial waste water and soil contamination. Raw fly ash does not have any appreciable cation exchange capacity. The prepared zeolite has a high cation exchange capacity of 457 meq/100g, comparable to that of commercial zeolites [9, 10]. Thus the prepared zeolite can find new dimension which allows the exchange of desired metal ions which facilitate the loading of complexes.

##### 3.1.2. BET surface area and pore size distribution of Fly ash zeolite

Typical Nitrogen adsorption isotherm along with the pore size distribution has been presented in **figures 1 and 2** respectively. The adsorption/desorption isotherm of Nitrogen for FAZ represents type I [11]. Since adsorption increases within a range, it indicates a definite growth in the number of micro pores, which is one of the defining features of zeolitic materials. The inflection in the Nitrogen isotherm around P/P<sub>0</sub>= 0.5-1.0 becomes sharper indicating narrower and uniform pore size distribution. From the Nitrogen adsorption isotherm data, surface area and pore diameter have been acquired. A surface area of 172.82 m<sup>2</sup>/g and pore volume of 0.1412 cm<sup>3</sup>/g clearly indicate that the material has a high order pore system. On the basis of the above mentioned data, it can be conjectured that the pores in the zeolites are uniform and can facilitate complexation in them. The crystallinity of the zeolites is reflected by the high surface area of the zeolites. The increase in surface area of fly ash zeolite (from ~20 m<sup>2</sup>/g in fly ash) is further an evidence for the formation of zeolite from fly ash. This provides room for the encapsulation of metal complexes in the pores of the zeolite.

##### 3.1.3. FT-IR analysis

Infra-red spectroscopy can yield information concerning structural details of the zeolite. In general, the IR spectrum can be split into two groups of vibrations (i) internal vibrations of framework TO<sub>4</sub> units which are insensitive to the structural vibrations and (ii) vibrations related to the external linkages of the TO<sub>4</sub> units in the structure which are sensitive to structural vibrations. The common features observed in the infra-red pattern of zeolites are asymmetric and symmetric stretch, double ring vibrations and T-O bending modes.

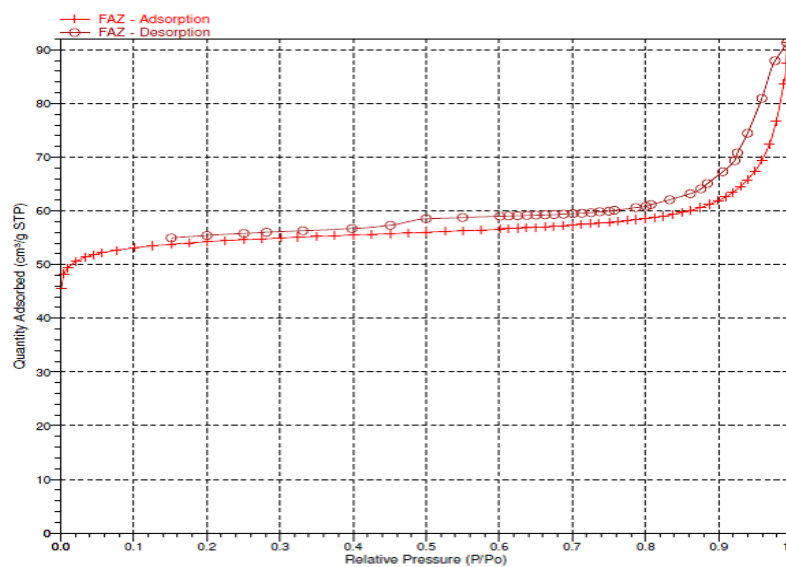


Figure 1: BET isotherm linear plot

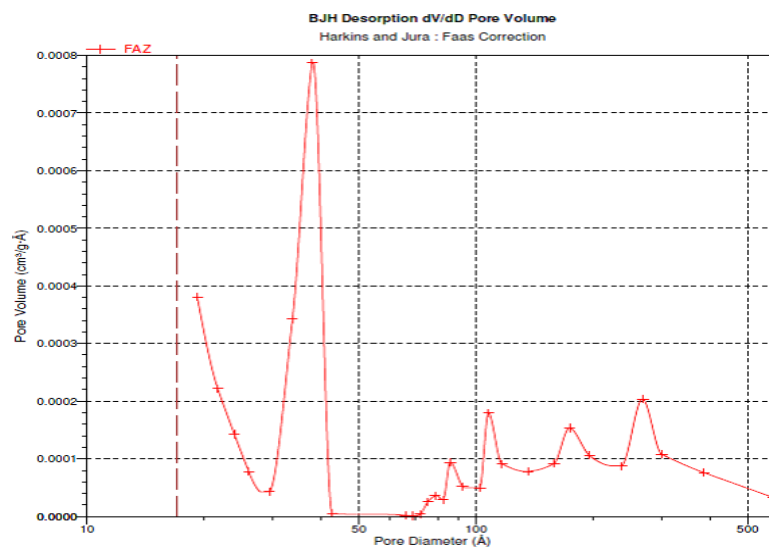


Figure 2: BJH desorption dA/dlog(D) Pore area

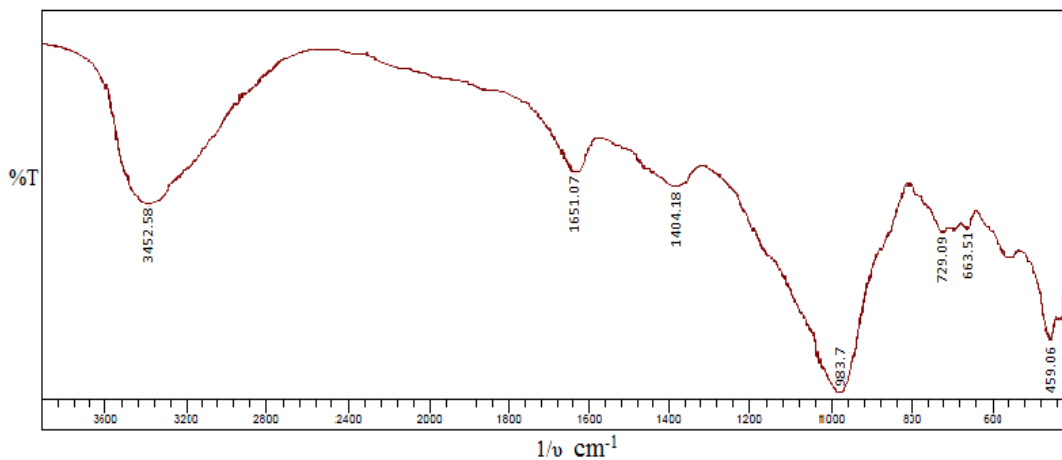
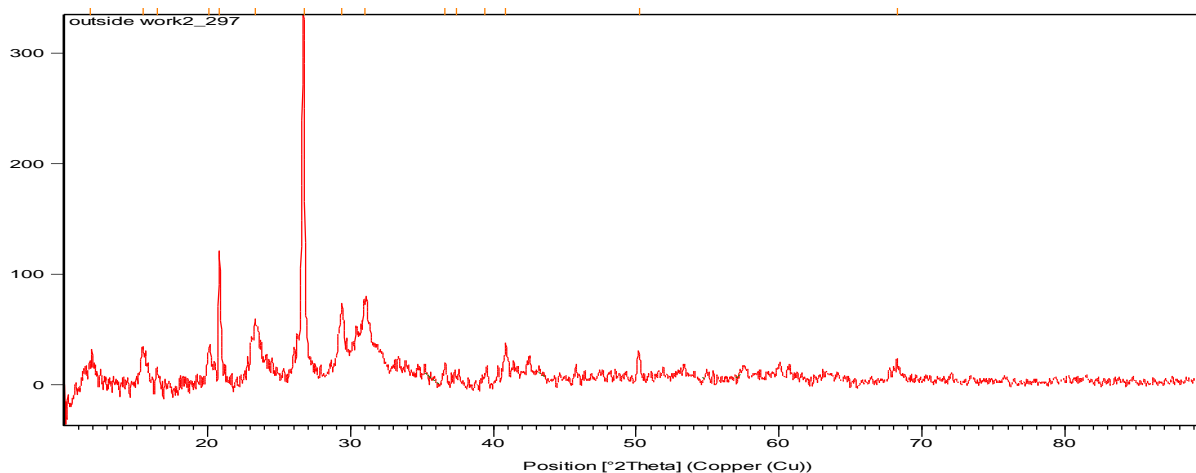


Figure 3: FT-IR spectrum of FAZ

The FT-IR of the synthesized FAZ is presented in **figure 3**. The most intense band at  $983\text{ cm}^{-1}$  is assigned to an asymmetric stretching of Si-O-Al [12, 13]. The mid infra-red region of the spectrum contains the fundamental framework vibration of  $\text{Si}(\text{AlO}_4)$  groupings. The band (hump) at  $1216\text{ cm}^{-1}$  represents the presence of substituted Al atoms in the tetrahedral forms of silica frameworks. All these observations confirm the formation of zeolites on alkali treatment of fly ash. The band at  $3452\text{ cm}^{-1}$  is attributed to the asymmetric and symmetric stretching vibrations  $\nu(\text{O-H})$  suggesting the presence of possibly hydrated aluminium silicates. The band at  $1651\text{ cm}^{-1}$  is attributed to the bending mode of water molecules [14].

#### 3.1.4. XRD analysis

The XRD pattern of FAZ is represented in **figure 4**. It reveals an amorphous-crystalline nature. A mild amorphous plateau and intensive diffraction reflections of crystalline phases can be observed. It is established that the crystalline portion is dominant. The characteristic peaks of the following crystalline phases could be identified by comparing the literature diffraction data. The most intensive peak on the zeolite diffractogram at  $2\theta = 26.739^\circ$  ( $d = 3.334\text{ \AA}$ ) and the peak at  $2\theta = 20.081^\circ$  ( $d = 4.421\text{ \AA}$ ) are attributed to  $\alpha\text{-SiO}_2$ . Hematite ( $\alpha\text{-Fe}_2\text{O}_3$ ), has diffraction peak at  $2\theta = 36.614^\circ$  ( $d = 2.454\text{ \AA}$ ). Mullite ( $\text{Al}_6\text{Si}_2\text{O}_{13}$ ) is characterized with main diffraction peaks at  $2\theta = 23.306^\circ$  ( $d = 3.813\text{ \AA}$ ),  $2\theta = 40.882^\circ$  ( $d = 2.207\text{ \AA}$ ) and  $2\theta = 18.259^\circ$  ( $d = 1.373\text{ \AA}$ ). The reflexes situated above  $55^\circ$  could be addressed to mullite. As the characteristic reflexes of the different constituents are situated very closely, it is difficult to associate them undoubtedly to an exact constituent [15]. The XRD pattern of FAZ matches with that of zeolite-X [16].



**Figure 4:** XRD pattern of fly ash zeolite

#### 3.1.5. Scanning Electron Microscopy

The SEM images of FAZ are presented in **figure 5**. The SEM images of FAZ show agglomeration of rough spheres of undefined shape confirming the formation of zeolites from fly ash [17-19]. A uniform orientation and morphology with single phase formation can be observed.

#### 3.1.6. XRF analysis:

The results of XRF analysis of the raw fly ash collected from Tuticorin Thermal Power Station and the zeolite prepared by hydrothermal treatment of fly ash are tabulated in **table 1**. The  $\text{SiO}_2/\text{Al}_2\text{O}_3$  ratio is 2.19 indicating the formation of X-type zeolite.

### 3.2. Characterization of Cu(II), Ni(II) and V(IV) metal complexes of imidazole encapsulated in fly ash zeolite [M(IMD)-X]

The loading of the transition metal complexes of imidazole in fly ash zeolite has been achieved by flexible ligand method and has been confirmed by several analytical techniques.

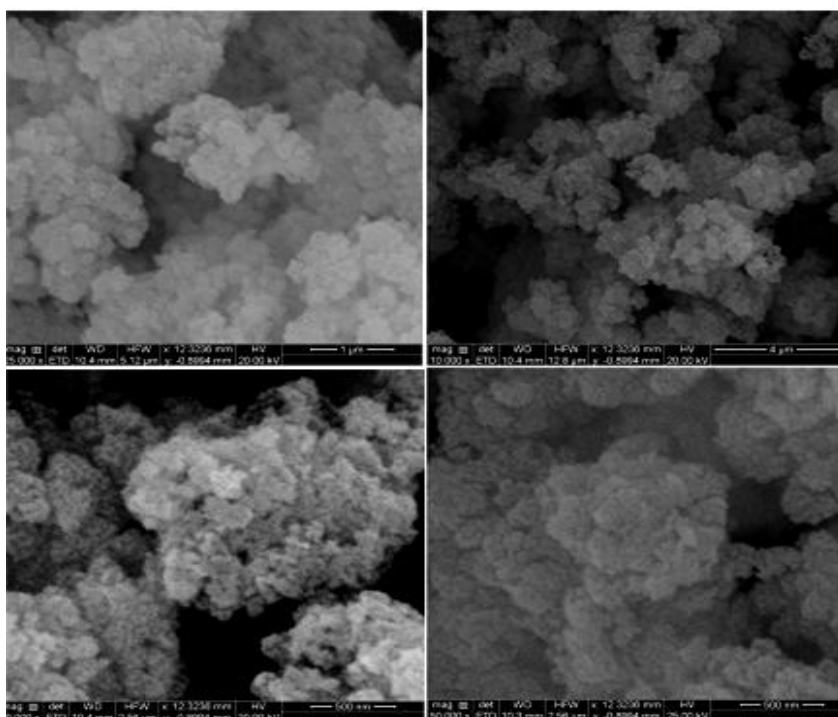


**Figure 5:** SEM images of FAZ

**Table 1:** XRF analysis of fly ash and FAZ

Constituent	Fly ash	Fly ash zeolite
SiO <sub>2</sub>	57.23	50.28
Al <sub>2</sub> O <sub>3</sub>	31.30	22.98
Fe <sub>2</sub> O <sub>3</sub>	4.72	3.83
MnO	0.02	0.03
MgO	0.62	1.14
CaO	1.19	1.16
Na <sub>2</sub> O	0.56	14.56
K <sub>2</sub> O	1.34	1.36
TiO <sub>2</sub>	1.84	2.56
P <sub>2</sub> O <sub>5</sub>	0.93	0.03

### 3.2.1. FT-IR analysis

FTIR spectra of metal-imidazole complexes encapsulated FAZ are presented in **figure 6**. In the FT-IR spectra characteristic absorption peaks of the imidazole-metal complexes are observed [20]. In the free imidazole ligand, C=N stretching frequency is observed at 1675 cm<sup>-1</sup> but in the imidazole metal complexes encapsulated in FAZ, the C=N stretching frequency is shifted to a lower range (Cu-IMD: 1668 cm<sup>-1</sup>; Ni-IMD: 1670 cm<sup>-1</sup>; V-IMD: 1668 cm<sup>-1</sup>). The N-H stretching frequency of free imidazole ligand is observed at 3451 cm<sup>-1</sup> [21], whereas two fairly strong bands at 3419 and 3203 cm<sup>-1</sup> for Cu(II) complex, 3317 and 3201 cm<sup>-1</sup> for Ni(II) complex and 3417 and 3197 cm<sup>-1</sup> for V(IV) complex are due to N-H stretching frequency [22-24]. As the N-H frequency is not shifted, the involvement of N-H group in the complex formation is ruled out. C-N stretching frequency in free imidazole is observed at 1250 cm<sup>-1</sup>, where as in the case of the encapsulated metal complexes it is observed at 1191 cm<sup>-1</sup>. This clearly proves the coordination of imidazole to metal ions through this N atom. The bands at 601 cm<sup>-1</sup> and

655  $\text{cm}^{-1}$  are assigned to C-H bending vibrations. The band at 746  $\text{cm}^{-1}$  is due to N-H wagging vibration. The band at 1542  $\text{cm}^{-1}$  in the free ligand due to the N-H in plane deformation vibration disappears in the encapsulated complexes. The peak at 1451  $\text{cm}^{-1}$  is assigned to the symmetric C=N-C=C stretching vibration.

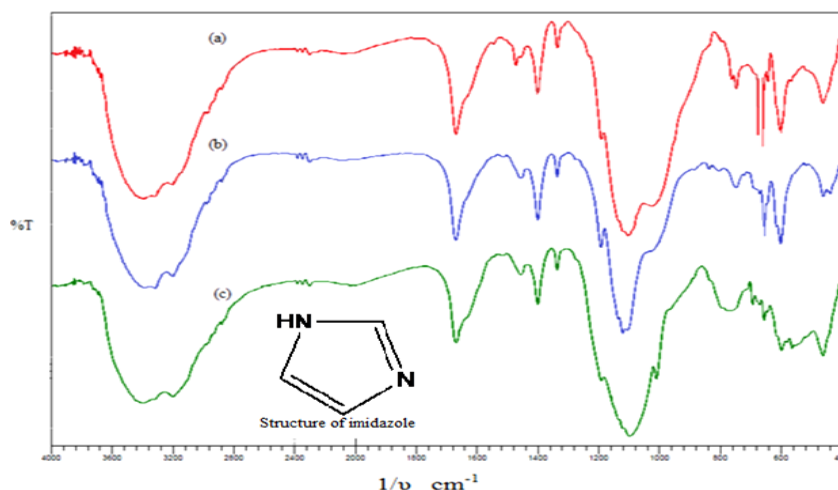


**Figure 6:** FT-IR spectra of (a) Cu-IMD encapsulated FAZ; (b) Ni-IMD encapsulated FAZ; (c) V-IMD encapsulated FAZ

The peak at 1400  $\text{cm}^{-1}$  in all the encapsulated metal complexes is due to  $\text{CH}_2$  scissoring vibration. The peak at 1336  $\text{cm}^{-1}$  is due to  $\text{CH}_2$  wagging in the encapsulated metal complexes. A distorted octahedral geometry can be expected where the four equatorial positions may be occupied by imidazole in a monodentate fashion. The remaining two axial positions may be occupied by silanolic  $-\text{OH}$  groups from the zeolite matrix [25, 26].

### 3.2.2. XRD analysis

The XRD patterns of the encapsulated metal complexes of imidazole are presented in **figure 7**. The 3 prominent peaks observed in XRD in the order of intensity are given in **table 2**.

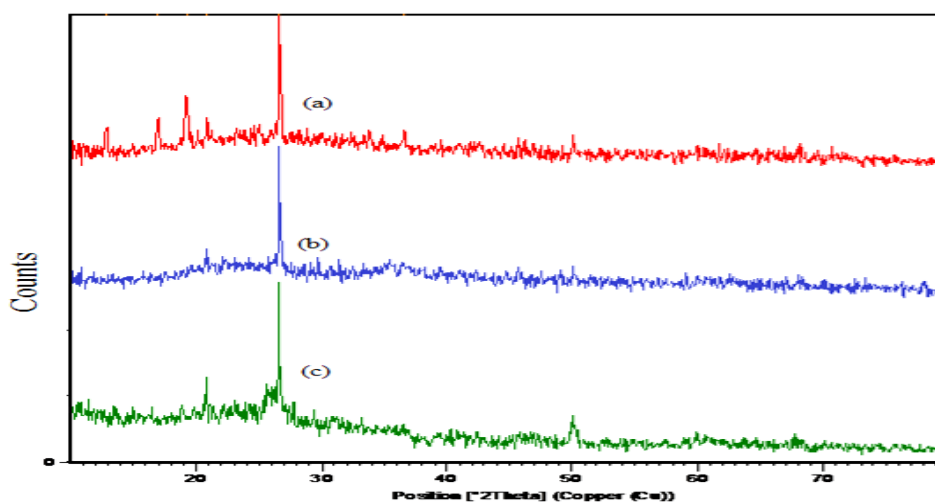


**Figure 7:** XRD patterns of (a) Cu-IMD encapsulated FAZ; (b) Ni-IMD encapsulated FAZ; (c) V-IMD encapsulated FAZ

It is difficult to exactly identify the peaks due to the presence of many metal oxides although it was reported to be X- type zeolite [27]. The peaks due to the metal complexes are not observed in the XRD patterns of the zeolite encapsulated metal complexes since the relative amount of the metal complexes is very low compared to the zeolite. Thus only the peaks due to zeolite are more prominent masking the low intensity peaks corresponding to

the metal complexes. No new peaks are detected in the XRD patterns which indicate the poor loading of the metal complexes in the zeolite. The peaks are unaffected which shows that the zeolite framework remains intact even after the encapsulation of the metal complexes [28].

**Table 2:** Prominent peaks in XRD of M(IMD)-X

Complex	2θ values
FAZ	26.73, 20.79, 29.40
Cu-IMD	26.64, 19.21, 16.95
Ni-IMD	26.62, 20.90
V-IMD	26.59, 20.80, 10.70

**3.2.3. Thermo gravimetric analysis**

The thermo grams of FAZ and the metal complexes encapsulated FAZ are given in the **figures 8-11** and the TGA data along with the percentage weight loss at different steps and their assignments are summarized in **table 3**.

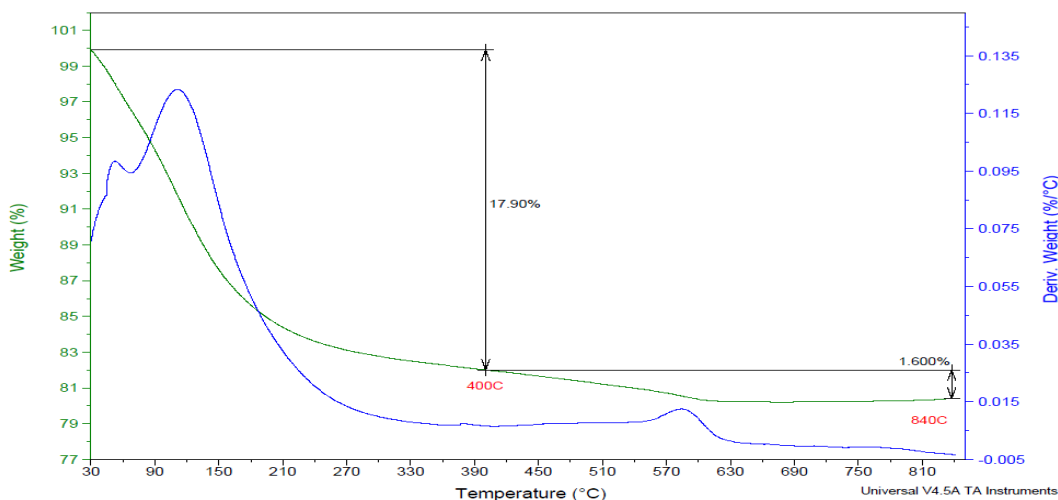


**Figure 8:** Thermo gram of FAZ

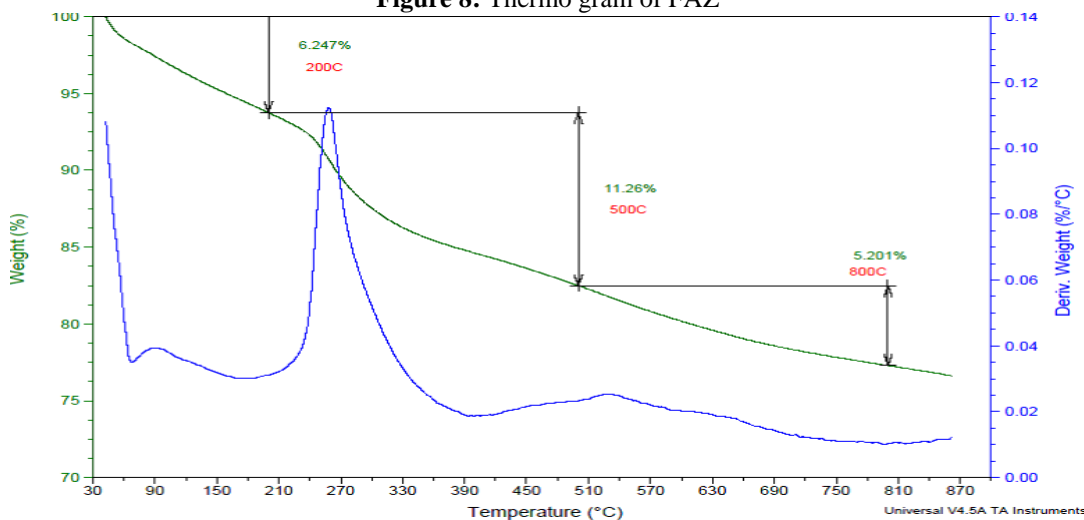


**Figure 9:** Thermo gram of Cu-IMD encapsulated FAZ

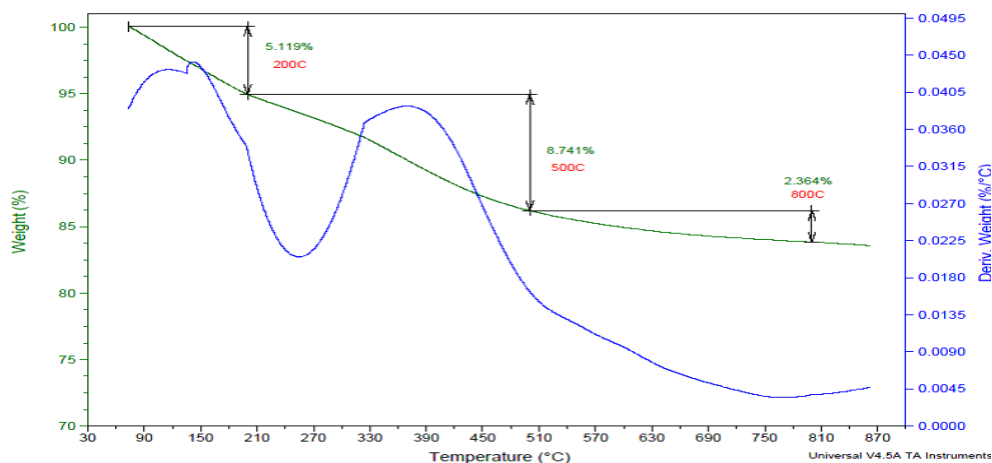


Figure 10: Thermo gram of Ni- IMD encapsulated FAZ

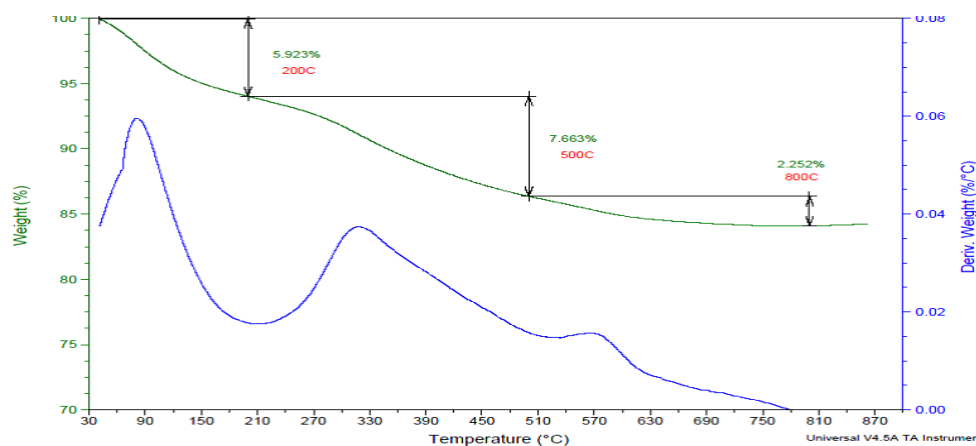


Figure 11: Thermo gram of V- IMD encapsulated complex

The first step of the thermo gram of the complexes indicates the loss of intrazeolite water followed by the decomposition of the lattice as well as co-ordinated water molecules simultaneously. In all the cases, the second weight loss corresponds to that of the complexes which have been found to decompose in the temperature range of 200-500°C. Literature reveals that the decomposition of imidazole occurs only after 200°C [29] which is in agreement with the thermo grams obtained for the metal imidazole complexes encapsulated zeolite.

Table 3: TGA weight losses for M(IMD)-X

Sample	Upto 200 <sup>0</sup> C	200-500 <sup>0</sup> C	500-800 <sup>0</sup> C
Zeolite	17.90%	-	1.60%
Cu-IMD	6.24%	11.26%	5.20%
Ni-IMD	5.12%	8.74%	2.36%
V-IMD	5.92%	7.66%	2.25%

The reports reveal that the metal complexes have been loaded from 2-11% which is in accordance with the low percent of metal content estimated by AAS. The thermal degradation of the metal complexes is observed by a clear weight loss between 200-500°C in all the cases. The third weight loss that is observed between 500 and 860°C is mainly due to the water loss formed by the condensation of silanol groups [30-32].

### 3.2.4. Atomic Absorption Spectrometry

Each metal complex encapsulated zeolite (50 mg) was dissolved in 20 mL of hydrofluoric acid (40%) and was analyzed by atomic absorption spectrophotometer. The report confirms the presence of the corresponding metal ions, (Cu: 14.2 ppm, Ni: 100.4 ppm), in the solution which further proves the encapsulation of the metal complex in the zeolite.

### 3.2.5. UV-Vis spectral analysis

The electronic spectra of the leached metal complexes and that of imidazole are presented in **fig. 12**. The absorbance measured at 206 nm for imidazole is due to the  $\pi \rightarrow \sigma^*$  transition of the C=N group on the imidazole ring.

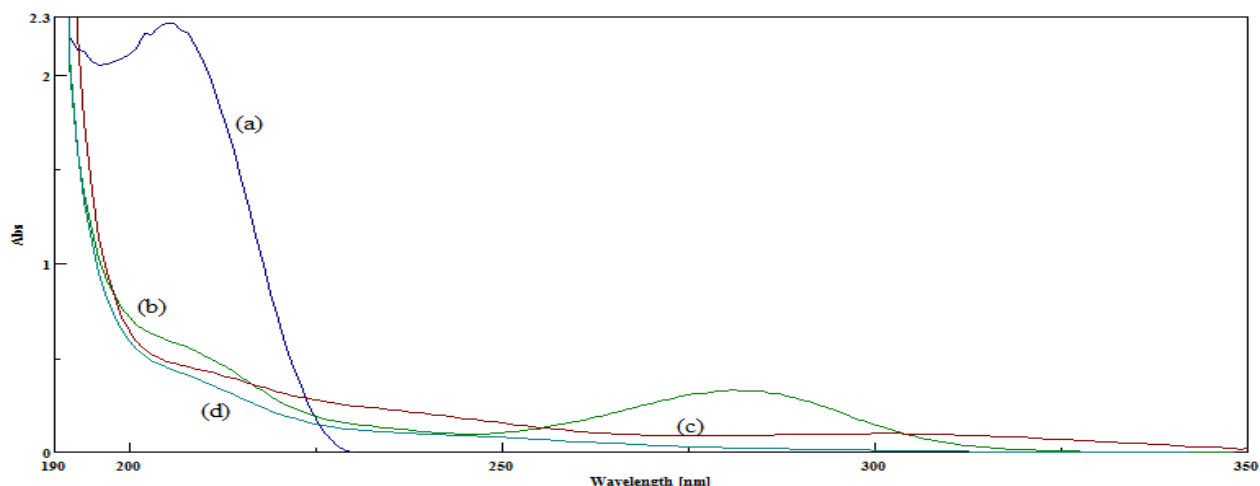


**Figure 12:** UV –Vis spectra of (a) IMD; (b) Cu- IMD encapsulated FAZ; (c) Ni-IMD encapsulated FAZ; (d) V-IMD encapsulated FAZ

Electronic spectra of the complexes studied exhibit broad bands in the ligand field region with maxima around 190 nm on the low-energy side. These ligand field spectra are indicative of an elongated pseudo-octahedral donor arrangement about the Cu(II) atom [33-36]. The band observed around 280 nm for all the metal complexes can be attributed to intra and inter ligand transitions which has merged with the metal-ligand charge transfer transitions ( $d_M \rightarrow \pi^*_{N\text{-ligand}}$ ) [37]. d-d transitions are not observed due to the very low concentration of the metal complexes in the leachate.

### 3.3. Catalytic activity

The % phenol conversion to hydroquinol for the encapsulated complexes varies with time in the order: Cu-IMD > V-IMD > Ni-IMD. **Figure 13** shows the variation in the extent of the reaction with respect to time. A higher extent of conversion is observed with an increase in time and finally tends to attain a constant value.

The % phenol conversion for all the zeolite encapsulated metal imidazole complexes are presented in **table 4**. Among the different transition metal complexes, the individual effects created by the metal complex play a dominating role in deciding the catalytic activity. This supports the active involvement of the incorporated metal complex in deciding the catalytic activity. A cooperative involvement of various factors like surface area, crystallite size, redox properties and the electron accepting properties may be the driving force for the reaction. Different mechanisms have been suggested to the reaction. **Scheme 1** shows a mechanism in which the zeolite framework catalyses the hydroxylation of phenol after the formation of the peroxo linkage. If this mechanism operates, the fly ash zeolite must exhibit higher activity. But in practice, the activity of the fly ash zeolite as such has not been detected. Thus the role of the metal complex in the cavity of the zeolite plays a very significant role in the hydroxylation of phenol.

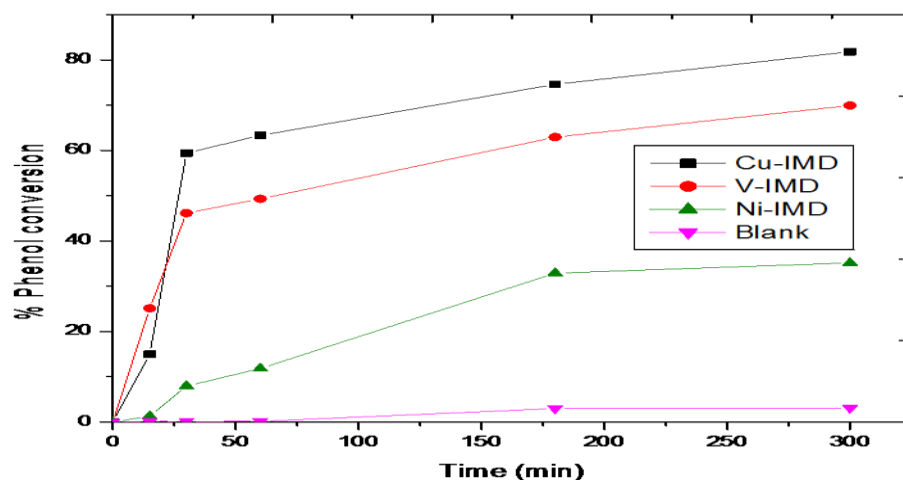
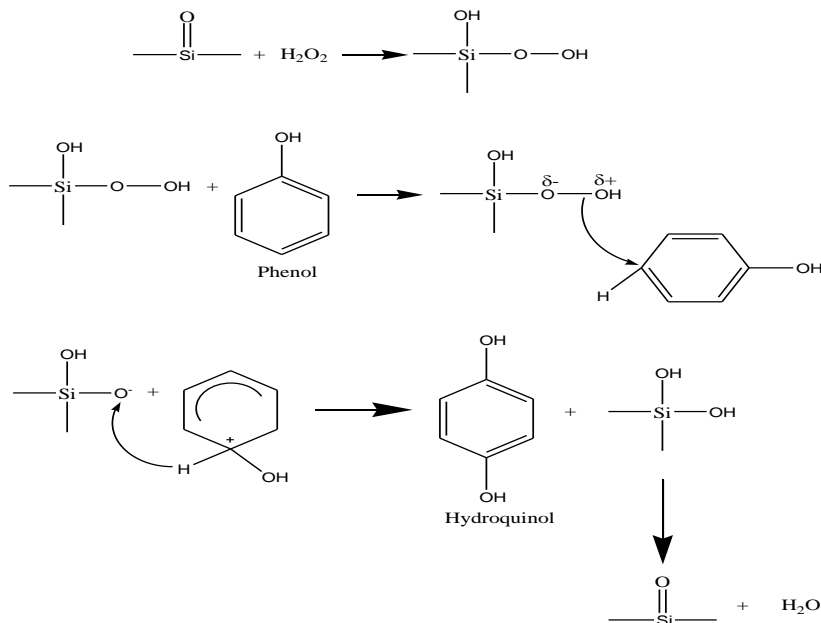


Figure 13: Variation of % phenol conversion as a function of time for M-IMD encapsulated complexes

Table 4: % conversion of phenol as a function of time for M(IMD)-X

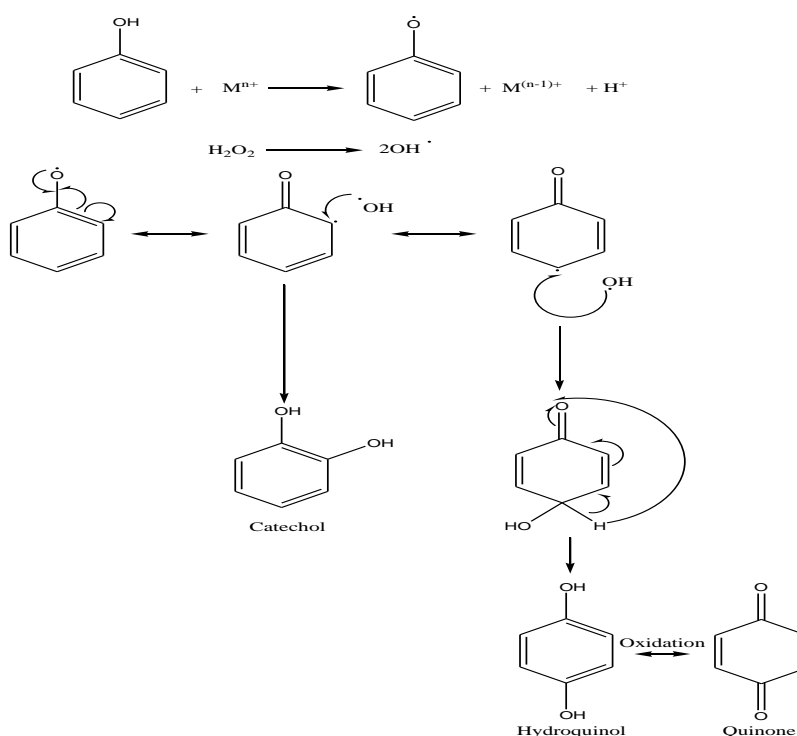
Sample	15 min	30 min	60 min	180 min	300 min
V- IMD	25.10	46.16	49.32	62.95	81.81
Cu-IMD	14.96	59.44	63.33	74.63	69.95
Ni-IMD	1.30	7.94	11.83	32.90	35.15
Blank	0.14	0.14	0.15	2.99	3.10



Scheme 1 Proposed mechanism for hydroxylation of phenol

A heterogeneous-homogeneous reaction mechanism has been proposed for the liquid phase oxidation over solid catalysts [38, 39]. The high susceptibility of the aromatic ring of phenols towards oxidation can be attributed to the possible generation of the delocalised aryloxy radical *via* the removal of a hydrogen atom. The generation of phenoxy radicals may occur on the catalyst surface. At the same instant, catalyst surface can also trigger the homolytic cleavage of hydrogen peroxide.

A general mechanism of the reaction taking zeolite encapsulated metal complex as the representative is sketched in **scheme 2**. The formation of catechol and hydroquinone is believed to occur *via* the attack of  $\text{OH}^-$  on the benzene ring. The formation of phenoxy radicals occurs at the catalyst surface after which the propagation of the reaction can occur either in the liquid phase or on the catalyst surface. Another important observation was the preferential formation of the *para* isomer (hydroquinol) in comparison with the *ortho* product, catechol. This may be a consequence of some sort of association between the phenoxy radicals and the catalyst surface. This leaves the *para* position more prone to attack by the hydroxy radicals generated on the catalyst surface. Steric considerations also predict the preferential formation of the *para* isomer. All the observed trends suggest that a free radical mechanism (**scheme 2**) is operating in this case. A further investigation into the course of the reaction is essential for a clear-cut prediction of the actual mechanism.



**Scheme 2** Proposed free radical mechanism for the hydroxylation of phenol

## Conclusions

A high profile application of fly ash to synthesise fly ash based zeolite is demonstrated. The surface area of the prepared FAZ has been found to be  $172.83 \text{ m}^2/\text{g}$ . The high surface area shows that it can be used as a cost effective substitute for commercial zeolites. Encapsulation of  $\text{Cu(II)}$ ,  $\text{Ni(II)}$  and  $\text{V(IV)}$  complexes of imidazole in the pores of zeolite-X synthesized from fly ash has been achieved by flexible ligand method and characterized by various physico-chemical techniques and spectroscopic studies which confirm the loading of the metal complexes in the pores of the prepared zeolite. The catalytic activity of the encapsulated complexes has been screened towards the hydroxylation of phenol and the product has been identified as hydroquinol by GC-MS. The extent of conversion of phenol to hydroquinol increases with time. Literature reports reveal promising catalytic applications of metal complexes in commercial zeolites. This work shows that loading of metal complexes in fly ash zeolite can also find applications in other catalytic transformations undoubtedly. In this prospect, they can be used as a catalyst towards various industrially significant reactions.

**Acknowledgments-** We express our sincere gratitude to National Geophysical Research Institute (NGRI), Hyderabad, India for XRF analysis, Department of Chemistry, IIT Madras for TGA and SPIC Science Foundation for GC-MS analysis.

## References

1. Haque E.M., *Internat. J. Waste Resources* 3(1) (2013) 22.
2. Ramamurthy V., Lakshminarasimhan P., Grey C.P., Johnston L.J., *Chem. Commun.* (1998) 2411.
3. Meinershagen J.L., Bein T., *J. Am. Chem. Soc.* 121 (1998) 448.
4. Sykora M., Maruszewski K., Treffert-Ziemelis S.M., Kincai J.R., *J. Am. Chem. Soc.* 120 (1998) 3490.
5. Raj I.V.P., Shaikh T.M., Sudalai A., *Acta Chim. Slov.* 57 (2010) 466.
6. Peter Amaladhas T., Sheeba Thavamani S., *Adv. Mat. Lett.* 4(3) (2013) 213.
7. Arun S., *Systematic Laboratory Experiments in Organic Chemistry*, 2nd edn. (New Age International, 2010) 825.
8. Jeffery G.H., Basset J., Mendham J., Denney R.C., *Vogel's textbook of quantitative chemical analysis*, 5<sup>th</sup> edn. (Longman Scientific & Technical, England, 1989), 408.
9. Amrhein C., Haghnia G.H., Kim T.S., Mosher P.A., Gagajena R.C., Amanios T., Torre L.D.L., *Environ. Sci. Technol.* 30 (1996) 735.
10. Bergaut V., Singer A., *Appl. Clay Sci.* 10 (1996) 369.
11. IUPAC Manual of Symbol and Terminology for Physicochemical Quantities and Units. Appendix II. Definitions, Terminology and Symbols in Colloid and Surface Chemistry. Part1. *Pure Appl. Chem.* 31(4) (1972) 579.
12. Davidova M., Nachtigalova D., Bulanek R., Nachtigall P., *J. Phys. Chem. B.* 107(10) (2003) 2327.
13. Gupta N., Kushwaha A.K., Chattopadhyaya M.C., *Adv. Mat. Lett.* 2(4) (2011) 309.
14. Charles A.G., *Eur. J. Mineral.* 24(3) (2012) 439.
15. Boycheva S., *J. Chem. Technol. Metall.* 47(2) (2012) 155.
16. Franus W., *Pol. J. Environ. Stud.* 21(2) (2012) 337.
17. Mimura H., Yokota K., Akiba K., Onodera Y.J., *Nucl. Sci. Technol.* 38(9) (2001) 766.
18. Belviso C., Cavalcante F., Fiore S., *Waste Manage. (Oxford)* 30(5) (2010) 839.
19. Pengthamkeerati P., Satapanajaru T., Chularuengsoaksorn P., *Fuel* 87 (2008) 2469.
20. Otting W., *Chem. Ber.*, 89 (1956) 2887.
21. Lane T.J., Nakagawa I., Walter J.L., Kandathil A.J., *Inorg. Chem.* 1(2) (1962) 267.
22. Davis J.W., Smith J., *J. Chem. Soc. A.* (1971) 317.
23. Hodgson B.J., Percy C.G., Thornton A.D., *Spectrochem. Acta. A* 35 (1979) 949.
24. Barbara M.O., Ewa R.S., Danuta M., *J. Mol. Struct.* 1028 (2012) 49.
25. Suaad T.S., *Iraqi National Journal of Chemistry* 36 (2009) 605.
26. Denis P.D., David M.M., Alistair J.L., *Inorg. Chim. Acta* 148 (1988) 173.
27. Ojha K., Pradhan N.C., Samanta A.N., *Bull. Mater. Sci.* 27 (2004) 555.
28. Bhagya K.N., Gayathri V., *J. Porous Mater.* 20(1) (2012) 257.
29. Omrani A., Simon L.C., Rostami A.A., Mousa G., *Thermochemica Acta* 468 (2008) 39.
30. Peter Amaladhas T., Sheeba Thavamani S., *Adv. Mat. Lett.* 4(9) (2013) 688.
31. Laobuthee A., Chirachanchai S., Ishida H., *Polym. Degrad. Stab.* 7(6) (2001) 1.
32. Olcay S., *Turkish J. Pharm. Sci.* 3(2) (2006) 61.
33. Kohout J., Hvastijova M., Jozef K., Diaz J.G., Valko M., Jager L., Svoboda I., *Inorg. Chim. Acta* 287 (1999) 186.
34. Hathaway B.J., Billing D.E., *Coord. Chem. Rev.* 5 (1970) 143.
35. Tabbi G., Giuffrida A., Bonomo R.P., *J. Inorg. Biochem.* 128 (2013) 137.
36. Hathaway B.J., *J. Chem. Soc., Dalton Trans.* (1972) 1196.
37. Malecki J.G., Maron A., *Polyhedron* 40 (2012) 125.
38. Meyer C., Clement G., Balaceanu J.C., *Proc. Jrd Int. Congr. On Catalysis* 1 (1965) 184.
39. Sadana A., Katzer J.R., *J Catal.* 35 (1974) 140.

(2016) ; <http://www.jmaterenvirosci.com/>